

Mobile Lattice-Coded Physical-Layer Network Coding With Practical Channel Alignment

Yihua Tan, Soung Chang Liew, *Fellow, IEEE*, and Tao Huang

Abstract—The original concept of physical-layer network coding (PNC) was first proposed in a MobiCom challenge paper in 2006 as a new paradigm to boost the throughput of wireless relay networks. Since then, PNC has attracted a wide following within the research community. A high point of PNC research was a theoretical proof that the use of nested lattice codes in PNC could achieve the capacity of a two-way relay network to within half bit. Many practical challenges, however, remain to be addressed before the full potential of lattice-coded PNC can be realized. Two major challenges are channel alignment of distributed nodes and complexity reduction of lattice encoding-decoding. This paper reports a first comprehensive implementation of a lattice-coded PNC system. Our contributions are twofold: 1) we design and demonstrate a low-overhead channel precoding scheme that can accurately align the channels of distributed nodes driven by independent low-cost temperature-compensated oscillators (TCXO); 2) we adapt the low-density lattice code (LDLC) for use in practical PNC systems. Our lattice-coded PNC implementation yields good throughput performance in static line-of-sight (LoS) scenario and mobile non-LoS scenarios.

Index Terms—Physical-layer network coding, two-way relay network, compute-and-forward, lattice codes, low-density lattice codes, channel alignment.

1 INTRODUCTION

THIS paper reports a first implementation of a lattice-coded physical-layer network coding (PNC) system on a software-defined radio (SDR) platform. We demonstrate the feasibility of mobile lattice-coded PNC with precise channel alignment and practical lattice encoder and decoder.

Conventional communication systems, such as Wi-Fi, drop packets when multiple nodes transmit simultaneously. Network protocols are then devised to avoid such “collisions”. Instead of shunning collisions, a relay in a PNC system turns overlapping signals into a network-coded message for forwarding to their target destination nodes [1], [2]. The target destination nodes then extract the original message embedded within the network-coded message using self-information or side information [1], [2].

PNC can double the throughput of a two-way relay network (TWRN), where two end nodes A

and B exchange messages with each other via a relay R. In TWRN, traditional time-division (TD) relaying requires four non-overlapping transmissions for node A to deliver a message to node B, and node B to deliver a message to node A (1. $A \rightarrow R$, 2. $R \rightarrow B$, 3. $R \leftarrow B$, 4. $A \leftarrow R$), as shown in Fig. 1a. Straightforward network coding (SNC) [3] only takes three non-overlapping transmissions by combining the two downlink transmissions into a single transmission (downlink: $A \leftarrow R \rightarrow B$), as shown in Fig. 1b. Specifically, in SNC, the relay broadcasts the sum of the messages of nodes A and B. Then nodes A and B can decode the message from the other end node by subtracting their own message from the sum. PNC further reduces the required non-overlapping transmissions to two, by letting nodes A and B transmit messages simultaneously to relay R (uplink: $A \rightarrow R \leftarrow B$), as shown in Fig. 1c. Relay R then decodes a network-coded message (a linear combination of the end nodes messages) from the overlapping signals and forward the network-coded message to nodes A and B (downlink: $A \leftarrow R \rightarrow B$). Upon receiving the network-coded message, each end node decodes the original message from the other end node by subtracting its own message from the network-coded message.

- Yihua Tan and Soung Chang Liew are with the Department of Information Engineering of the Chinese University of Hong Kong, N.T., Hong Kong.
- Tao Huang was a visiting RA at the Institute of Network Coding of the Chinese University of Hong Kong. He is with Nanjing University, China.

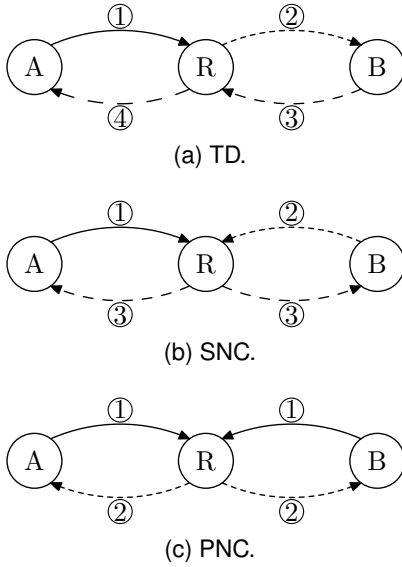


Fig. 1. Relaying schemes in TWRN.

Besides relay networks, PNC can also boost the performance of non-relay multiple access networks [4], [5].

It has been 10 years since the concept of PNC was first proposed in MobiCom 2006 [1]. Since then, PNC has become a subfield of network coding with a wide following. A highlight was a theoretical proof that lattice-coded PNC could achieve the information-theoretical capacity of TWRN to within half bit [6]. Despite the many years that elapsed, most PNC research has remained theoretical. Although a few experimental PNC prototypes have been demonstrated to date [4], [5], [7], [8], [9], [10], [11], these prototypes adopted low-order BPSK and QPSK modulations. None of them makes use of “real” lattice coding to realize the full potential of PNC in the high signal-to-noise ratio (SNR) regime. This paper is an attempt to fill this gap, and by doing so, it paves the way for practical high-throughput PNC systems going forward. We have solved a number of practical challenges, as overviewed below:

Channel alignment with low-cost commercial oscillators without reference synchronization signal: For optimal performance of lattice-coded PNC, the channel from node A to relay R and the channel from node B to relay R must be aligned. This is to facilitate the extraction of a network-coded message from the overlapping signals at relay R. In a mobile network, the channels vary dynamically with time. Moreover, unsynchronized low-cost oscillators in general have large carrier frequency offsets (CFO) among them, which can induce a relative phase rotation of more than 2π between

the overlapping signals within a packet duration. The CFO is not only large, but also keeps changing: quick and accurate estimation of the CFO is important. Some prior works dealt with these problems with reference signals, using extra antenna, extra time, and/or extra bandwidth [12], [13], [14]. We show that phase alignment can be achieved even when the nodes are driven by independent inexpensive temperature-compensated crystal oscillators (TCXO), without the need for expensive oscillators (e.g., oven-controlled crystal oscillators (OCXO) or Global Positioning System disciplined oscillators (GPSDO)), shared clocks, or a common reference frequency between nodes A and B. To enable timely channel feedback of channel state information (CSI) for precoding, we implemented the time-critical functions within the FPGA hardware of our SDR testbed. In our system, the relay estimates and feedbacks the CSI to nodes A and B with an overall feedback delay (from estimation to precoding) less than $0.5ms$. In addition, our packet format with preambles and postambles enables CFO estimation that is 100 times more accurate than the conventional preamble-only approach in IEEE 802.11 systems.

Time-slotted regulated transmission and proactive phase adjustment: For orthogonal frequency-division multiplexing (OFDM) PNC, the relative phase offset of the same subcarrier of nodes A and B depend on the difference in the arrival times of their packets at the relay (i.e., the relative phase offset of a subcarrier depends on the arrival-time offset of the two packets). Prior PNC implementations [4], [5], [8] let the relay broadcast beacons to trigger nodes A and B to transmit uplink packets together, but this beacon-trigger method cannot control the exact transmission times, causing changes to the arrival-time offset for successive uplink transmissions. This uncertainty of the arrival times will invalidate the phase precoding, because the relative phase offsets of the previous uplink transmissions may not reflect the relative phase offset of the current uplink transmissions. To remove uncertainty in arrival-time offset, we built a time-slotted system to let the end nodes transmit according to their local timers after an initial synchronization process. Then changes in arrival-time offset mainly come from sampling frequency offset (SFO), and this can be taken care of by our SFO precoding. Meanwhile, the sample shifts caused by SFO can accumulate and make the arrival-time offset be larger than the cyclic prefix (CP) of the OFDM system. We deal with this problem by letting the relay inform the lagging

node to advance the sending of its packets (i.e. adjusting its time-slot boundary) once in a while. The node, besides, advancing the sending of its packets, also proactively introduces a corresponding phase precoding on each of its subcarrier to nullify the phase offset introduced by the advancement of its arrival times. In short, with our new method, we can both predict and proactively control the relative phase offset of the system.

Minimal overhead of signaling and feedback: Lowering the overhead of signaling and feedback in a precoding system is very important to make the system practical. Our packet format has the same overhead as that of IEEE 802.11, incurring no extra overhead. Our precoding scheme uses a very simple protocol that does not require complicated signaling for timing synchronization and channel estimation. Moreover, our precoding scheme only requires the relay to *feedback partial uplink phase and amplitude* information to the end nodes, where reciprocity is employed to construct the complete uplink phase and amplitude based on downlink measurement. We emphasize that, fundamentally, feedback cannot be totally eliminated and reciprocity will not work by itself in terms of the construction of the complete uplink phase and amplitude information (this is shown in Section 3 of this paper). With our partial feedback scheme, the amplitude feedback overhead is cut by 98%, and the phase feedback overhead is cut by 96% compared with the complete feedback scheme. The feedback overhead in our partial feedback scheme is negligible relative to the data payload. The phase error only increases slightly compared with the case with full feedback.

Practical lattice encoder and decoder: Our system makes use of low-density lattice codes (LDLC) [15], [16], [17]. To our best knowledge, this is a first implementation of a lattice-coded communication system (PNC or non-PNC). For our PNC system, despite the highly accurate channel precoding, the lattice PNC decoding algorithm will still need to handle the small residual channel misalignment that varies within a packet. Such small but changing misalignment is unavoidable in practical systems. Prior theoretical studies of lattice PNC decoding did not take into account the *changing* relative phase offset between the overlapping signals within a packet. We designed a novel LDLC decoder to deal with the varying residual channel misalignment. In addition, our lattice encoder and decoder incorporate lattice shaping to control the powers of lattice codewords, a must in practice due to the limited dynamic range of amplifiers. We also devised a fixed-complexity

lattice shaping method to reduce computation required for shaping and decoding.

2 MAIN RESULTS AND IMPACTS

This paper focuses on the uplink because for PNC performance, the uplink is the critical part—the downlink does not require channel alignment and is just ordinary multicast communication [18]. Channel alignment is very important for good performance in PNC. Channel misalignment lowers the achievable rates [19]. Fig. 2 shows the overlapped signals received by the relay when both end nodes use 16-quadrature amplitude modulation (16-QAM) over OFDM without channel alignment. The unaligned constellation makes it difficult to decode a network-coded message out of the overlapped signals. Unlike in single-user point-to-point communication, the relay here cannot compensate for the channel misalignment in the received signal, because compensating for the channel misalignment of one end node inevitably leads to an uncompensated channel misalignment of the other end node. What matters is the relative misalignment of the channel from node A to relay R and the channel from node B to relay, not their individual channel (phase) misalignments with respect to the receiver.

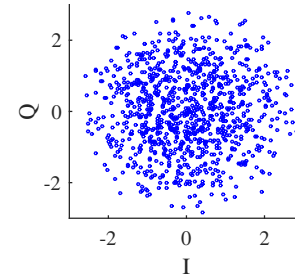


Fig. 2. Constellation of channel-misaligned 16-QAM PNC.

We built a channel precoding system to align the channels. Fig. 3 shows typical constellations of all subcarriers of the received signals of 16-QAM PNC, achieved using different configurations in our precoding system: 1) use OCXO (Figs. 3a and 3b) or TCXO (Figs. 3c and 3d); full-feedback method: feedback phases of all subcarriers (Figs. 3a and 3c) or partial-feedback method: only feedback the phases of 2 subcarriers out of 52 subcarriers (Figs. 3b and 3d). We use 16-QAM to illustrate our point here because the high-dimensional lattice codes actually used in our lattice-coded PNC system are hard to visualize. The 4×4 16-QAM of the two end nodes becomes 7×7 49-QAM at the relay when the overlapped signals are perfectly aligned. From

Figs. 3c and 3d, we see that even with inexpensive TCXO, our system can still achieve good channel alignment. From Figs. 3b and 3d, we see that our partial-feedback method only compromises the phase alignment slightly.

In Fig. 4, we compare the empirical cumulative distribution function (CDF) of the above four configurations. Fig. 4a plots the CDF of the phase misalignment between the two end nodes to characterize the overall phase precoding accuracy. Fig. 4b plots the CDF of the phase-misalignment deviation (with respect to the misalignment of the first symbol) within a packet to characterize the misalignment drifts within a packet the CFO precoding accuracy. These figures are obtained based on the statistics of the samples of more than 1,000 packets, without any smoothing.

In Fig. 4, we compare the empirical cumulative distribution function (CDF) of the above four configurations. Fig. 4a plots the CDF of the phase misalignment between the two end nodes to characterize the overall phase precoding accuracy. Fig. 4b plots the CDF of the phase-misalignment deviation (with respect to the misalignment of the first symbol) to characterize the misalignment drifts within a packet. These figures are obtained based on the statistics of the samples of more than 1,000 packets, without any smoothing.

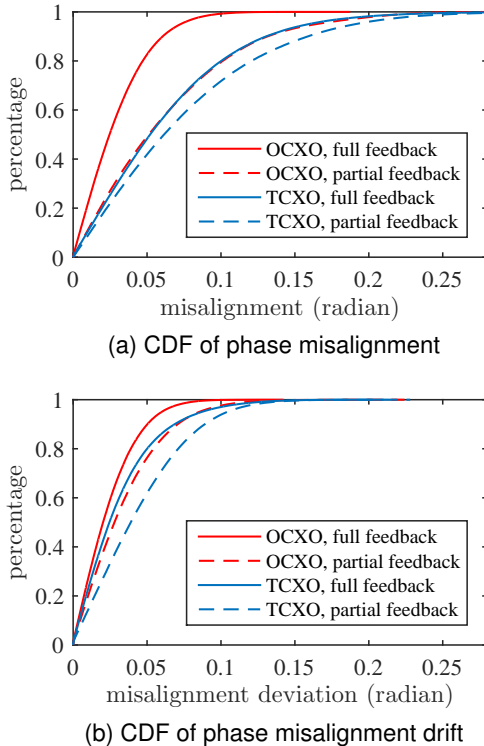


Fig. 4. Empirical CDF of phase misalignment between the two end nodes in experiments, using different configurations.

Although using TCXO cannot achieve the same phase-alignment accuracy as using OCXO, the residual misalignment is small that we can deal with it by special lattice decoder designs. We use TCXO and partial-feedback method for the experiments in the remainder of this paper because our ultimate aim is a practical inexpensive PNC system.

Compared with TD and SNC, although PNC requires fewer transmissions, its performance is sensitive to phase misalignment and if the phases are not aligned to a large extent, it may be able to support less dense signal constellations only—this will affect the amount of information delivered per transmission. In other words, a PNC system may potentially perform worse than TD and SNC in terms of throughput if the channels of the two end nodes are not properly aligned. Our experiment results in Section 5.2 show that with our channel precoding system, PNC can achieve lower bit error rate (BER) than TD and SNC for the same end-to-end data delivery rate ($A \rightarrow B$ and $A \leftarrow B$). This experiment justifies PNC as a practical communications scheme.

In addition to building the channel precoding system with desirable attributes (low cost, resource saving, low overhead, simple protocol, etc.), we also redesign lattice encoders and decoders to address practical considerations in PNC, including a) power control through lattice shaping, b) reduction of computation complexity caused by lattice shaping, and c) consideration of the small but varying post-precoding residual channel misalignments within a packet. Considerations a) and b) are also relevant to non-PNC systems, and by taking them into account, we have also moved the general application of lattice codes a step closer to practice.

For traditional point-to-point communication, lattice codes allow the system to achieve the capacity of AWGN channel [20]. However, there are also other good codes that allow the AWGN channel capacity to be achieved with lower complexity (e.g., LDPC). As a result, practical point-to-point communication systems seldom adopt lattice codes. For PNC, to our best knowledge, there has been no work showing codes other than lattice codes can allow the capacity of the two-way-relay channel to be achieved. Thus, lattice-coded PNC occupies a unique place as far as communication theory goes. That said, many practical challenges remain to be solved before lattice-coded PNC can become practical.

A practical challenge to lattice codes is that its decoding in general has exponential complex-

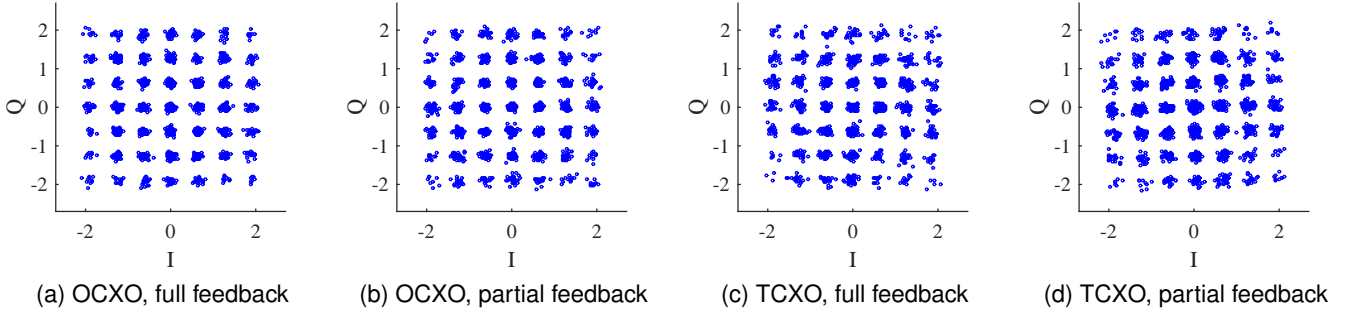


Fig. 3. Constellations of channel-aligned 16-QAM PNC, with different subcarriers plotted on the same figures.

ity. Low-density lattice codes (LDLC) [15], [17] is a new type of lattice codes with a sparse parity check matrix. LDLC can be decoded using the belief propagation (BP) algorithm in linear complexity, and systems using LDLC have been proved theoretically to be able to approach the capacity of the AWGN channel. The lattice encoding-decoding of our paper is built upon the theory in [15], [17], with modifications to address practical issues in PNC. Although our channel precoding scheme can align the channels to a large extent, small residual channel misalignments still remain. Furthermore, due to phase noise and tiny residual CFO and SFO, the residual channel misalignment may vary within a packet duration. To our best knowledge, all the theoretical work on lattice-coded PNC [21], [22], [23], [24] to date assume the channels to stay constant within a packet. In our system, the relay keeps track of the channel variation using the pilot subcarriers. The relay takes into account the intra-packet channel variation when decoding a network-coded message. In addition, we use a fixed-complexity lattice shaping method to control the power of lattice codewords. This method has low shaping/decoding complexity and incurs only small performance loss compared with other high-complexity methods.

2.1 Related Work

The authors of [25] implemented a simplified lattice-coded PNC with QPSK modulation and RS code. However, the QPSK-RS code is still a conventional block code, and this system does not realize a lattice-coded PNC in its true spirit. In lattice codes, modulation and channel coding are combined into one n -dimensional operation, where n is the number of symbols in the codeword. Such a lattice-coded PNC system has been shown to approach the cut-set bounds of TWRN to within

1/2 bit [6]. The QPSK-RS code in [25] differs from lattice codes in its construction and performance: it adopts a conventional approach in which the message is first channel-coded into discrete symbols, and then the symbols are modulated one by one in an independent manner (i.e., the modulation is a one-dimensional operation repeated n times). Also, [25] did not implement channel precoding (i.e., the channels can be misaligned, resulting in performance loss), and just used GPSDO to ensure synchronization of the oscillators.

Compute-and-forward (CF) [21] is a variant of PNC that aims to compute an integer-coefficient linear combination of the end nodes' messages. Refs. [26], [27] analyzed the performance of CF [21] using LDLC. Their simulation studies were limited to scenarios with perfect phase alignment, without considering how it could be achieved. Without channel alignment, although one can in principle still implement CF by customizing the coefficients of the linear combination to the relative phase offset (assuming phase offset is constant throughout a packet), the overall rate performance of the system will be far from that of channel-aligned lattice-coded PNC [19]. Furthermore, constant phase offset is an assumption that may not hold in practice.

Channel alignment is also a problem that needs to be addressed in distributed multi-user (MU) MIMO systems. In AirSync [13], a master access point transmits an out-of-band reference signal to continuously calibrate the phases of slave access points. AirShare [14] used a reference signal, but it differs from AirSync in that the reference signal is an analog clock signal. Sending continuous out-of-band reference signals requires extra bandwidth and/or antennas. In contrast, our channel precoding mechanism in PNC achieves good channel alignment without the need for extra bandwidth or antennas.

IAC [28] implemented a system of interference alignment and cancellation. In IAC, what matters is the relative phases between the multiple antennas of each client, not the absolute phase observed on each antenna. Since CFO creates the same phase rotation to the antennas of the same client, the relative phases between the antennas do not change. Therefore, CFO is immaterial as far as IAC is concerned. By contrast, what matters to PNC is the relative phase offset between the two distributed nodes driven by independent oscillators. Unlike IAC, our PNC system has to precode the CFO very accurately to maintain phase alignment.

JMB [12] used an extra wireless node to transmit a reference signal to adjust the phases of different nodes in MU-MIMO. We do not use an extra wireless node for such a purpose in our PNC system. The protocol of JMB requires rounds of uplink-downlink information exchange for each single-transmission period, incurring high signaling overhead. Our system has low overhead thanks to our simple time-slotted protocol and partial-feedback scheme. Another important difference is the assumption of JMB that CFO does not change significantly over time. We find this assumption to be invalid when TCXO is used.

Argos [29] presented a base station architecture in which a large number of antennas serve many terminals through multiuser beamforming. Argos exploits channel reciprocity to let the base station estimate the channels of multiple antennas relative to a reference antenna without any feedback. Although Argos performs beamforming assuming reciprocity, a fundamental difference with our work is that they used a shared clock to synchronize all the antennas on the base station. This is not practical for PNC where the nodes to be channel-aligned are located at different positions. Ref. [30] applied the idea of reciprocity-based relative channel estimation to MU-MIMO to reduce the required CSI feedback in a network with multiple access points connected by a wired backhaul network. However, the assumption of wired backhaul is not valid for PNC.

Ref. [31] addressed the complexity of signal processing in large-scale MIMO networks. In the future when we extend our PNC system to the many-user scenario (e.g., $N \times N$ CF, network-coded multiple access), similar consideration will be needed.

ANC [32] implemented a simplified version of PNC by amplify-and-forward. ANC does not require channel alignment because the relay does not decode. However, this approach suffers from

performance loss because noise is amplified along with the signals and it cannot approach the capacity of TWRN.

In Section 3.6, we will make an overall comparison between our precoding system and the precoding systems in some of the prior work above.

Last but not least, we remark that the channel alignment in PNC is more challenging than that in distributed MIMO, because in PNC the constellations of multiple users are superimposed, resulting in a much denser constellation. For PNC, the dense but aligned constellation is needed to facilitate the computation of a network-coded message at the relay, while distributed MIMO only needs to null out unwanted interferences.

3 PRACTICAL CHANNEL ALIGNMENT

Our channel precoding system precodes amplitude and phase based on channel reciprocity. Specifically, the amplitudes of the downlink subcarriers are estimated and used to precode the uplink subcarriers to equalize the amplitudes of all subcarriers. In particular, the relay only needs to feedback an overall amplitude to each end node to balance their receive powers at the relay (i.e., there is no need to feedback the amplitudes of all uplink subcarriers to the end nodes). This greatly reduces the amount of feedback information required.

Unfortunately, the same technique cannot be used for phase precoding. This is because, unlike amplitudes, an end node cannot derive the uplink phase of a subcarrier from the downlink phase of the same subcarrier—the reason for that will be elaborated later. Nevertheless, as will be demonstrated, a method that exploits reciprocity to reduce phase feedback to a minimal amount is still possible.

In the following, Section 3.1 discusses amplitude precoding, and Sections 3.2 to 3.5 discuss phase precoding. Section 3.6 compares our precoding system with the precoding systems in some prior work.

3.1 Reciprocity-Based Amplitude Precoding

To keep the amplitudes of different end nodes aligned throughout a packet, the amplitude precoding in PNC has to balance the powers of the signals of the end nodes for each and every subcarrier. To achieve overall power balance, the relay feedbacks an amplitude scaling factor to each end node to precode its average power. To equalize the amplitudes of different subcarriers, we exploit channel reciprocity and let each end node precoding its uplink

amplitudes according to the amplitudes of the received downlink packets. The next paragraph gives experimental results demonstrating the viability of amplitude precoding based on reciprocity.

Fig. 5 shows the amplitudes of an uplink packet and a downlink packet transmitted one after another in an experiment. Note that subcarrier $k = 0$ is unused DC and subcarriers $k = 27 \sim 37$ are the null guard band; thus these subcarriers have near-zero amplitudes. We can see that the channel amplitudes of the uplink and the downlink are reciprocal to a large extent. The slight difference of the channel amplitudes of the uplink and downlink is due to the circuit difference of the TX paths and RX paths of nodes A and B. Because the amplitude differences induced by circuits are very stable, we perform an initial calibration to find a scaling factor ρ_k for each subcarrier k such that the products of ρ_k and the downlink amplitudes are proportional to the uplink amplitudes. Precoding the uplink amplitudes using the downlink estimates and ρ_k , we can equalize all subcarriers so that their amplitudes are almost the same, as shown in Fig. 6.

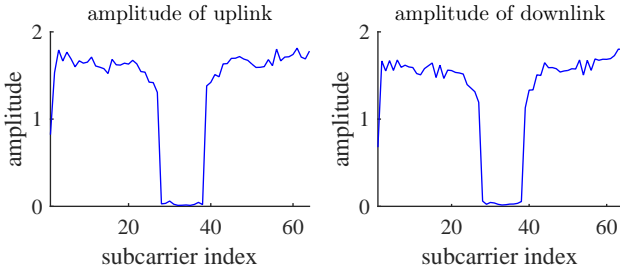


Fig. 5. Amplitudes of the uplink and the downlink channels.

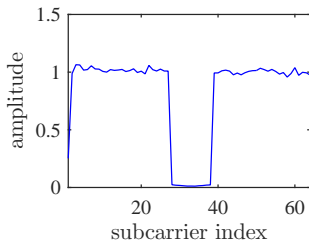


Fig. 6. Equalized Amplitude.

3.2 Difficulties in PNC Phase Precoding

A most challenging aspect of the phase precoding system is that the baseband channels are not static and may vary over time, due to several factors:

1) **The changes of physical air channels**, due to mobility and environment.

2) **The large and varying CFO**, due to the use of independent RF oscillators at the two end nodes.

3) **The packet-to-packet arrival-time jitters**, due to imperfect synchronization of the packet transmission times at the two end nodes.

4) **The phase reciprocity of the uplink channel and the downlink channel does not work without regular feedback**, even with initial calibration.

The impact of the first two factors on phase variation over time, hence how frequent phase re-estimation needs to be performed, is obvious. That of the last two factors is less so. The remainder of this subsection will elaborate on the third factor. The fourth factor will be detailed in Section 3.5.

The beacon-triggered mechanism of the prior implementations of non-precoded OFDM PNC systems [4], [5], [8] suffers from *unaccounted* packet-to-packet arrival-time jitters. In these implementations, the relay sends a beacon packet to trigger the end nodes to transmit uplink packets simultaneously. The synchronization/alignment requirement was loose in these systems: the arrival time of the later packet only needs to be within the cyclic prefix (CP) of the earlier packet [8], [18]. The beacon-triggered mechanism can easily meet the within-CP requirement, but a misalignment of one sample may be inevitable due to the resolution of arrival-time estimate at the end nodes.

Within-CP arrivals, however, is not good enough for the precoded PNC, because varying phase offset from subcarrier to subcarrier can be induced by tiny misalignment of arrival times. We give an example to illustrate the problem. In Fig. 7, suppose that in the first uplink transmission the packets of the two end nodes are perfectly aligned in the time domain, but in the second transmission they are separated by one sample. The relay estimates the CSI from the first transmission, and feedbacks the CSI to nodes A and B for their precoding. However, the feedback CSI is invalid for the second transmission, because the time-domain alignment is different from the last time and will effectively introduce a different set of phase offsets from subcarrier to subcarrier in the frequency domain. Note that the relay cannot compensate for this channel change by adjusting the CP-cut position. Specifically, for a PNC system, the relay cannot compensate for the channels of the two users at the same time: compensating for one inevitably leads to an uncompensated channel of the other.

We now explain the fourth factor. For simplicity, let us focus on a particular subcarrier. Denote the uplink phase the subcarrier at time t by $\theta_{\text{up}}(t)$,

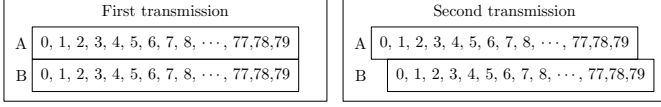


Fig. 7. Packet-to-packet arrival-time jitters.

and the downlink phase by $\theta_{\text{dn}}(t)$. The changes of the uplink phases and downlink phases from time t_1 to time t_2 are caused by 1) reciprocal change of physical channel, denoted by $\gamma(t_1, t_2)$, and 2) opposite change due to clock difference (CFO, SFO, and phase noise), denoted by $\eta(t_1, t_2)$ for the uplink and thus $-\eta(t_1, t_2)$ for the downlink. We therefore have

$$\theta_{\text{up}}(t_2) = \theta_{\text{up}}(t_1) + \eta(t_1, t_2) + \gamma(t_1, t_2) \quad (1)$$

and

$$\theta_{\text{dn}}(t_2) = \theta_{\text{dn}}(t_1) - \eta(t_1, t_2) + \gamma(t_1, t_2). \quad (2)$$

Suppose that the time t_1 is the initial calibration time, when the end node measures $\theta_{\text{dn}}(t_1)$ and the relay feedbacks instantaneous $\theta_{\text{up}}(t_1)$. At a later time t_2 , a question is whether the end node can derive the uplink phase $\theta_{\text{up}}(t_2)$ from the initial $\theta_{\text{dn}}(t_1)$, $\theta_{\text{up}}(t_1)$, and the downlink phase $\theta_{\text{dn}}(t_2)$ measured at t_2 without any feedback.

It can be easily seen that this is impossible because in the two equations (1) and (2) we have three unknowns $\theta_{\text{up}}(t_2)$, $\eta(t_1, t_2)$, and $\gamma(t_1, t_2)$. In other words, from the two equations, we cannot resolve $\theta_{\text{up}}(t_2)$. Although we can use estimated CFO and SFO to estimate the cumulative phase change $\eta(t_1, t_2)$, the estimation error of $\eta(t_1, t_2)$ and thus the estimation error of $\theta_{\text{up}}(t_2)$ will grow over time as t_2 increases, and the phase precoding will fail soon. That is, any tiny errors in the estimated CFOs and SFOs will accumulate in the estimated phase change $\eta(t_1, t_2)$ over time unless we “reset” the phase once in a while by feedback of the uplink phase measured at the relay.

In a nutshell, using only information from (1) and (2) does not work and we also need feedback after the initial calibration of $\theta_{\text{dn}}(t_1)$ and $\theta_{\text{up}}(t_1)$. Given that we have many subcarriers, each with a phase, feedback overhead may be large. Fortunately, we can use reciprocity to reduce the feedback overhead if the cumulative phase errors are due to CFO rather than changes in the physical air channel (note: the phase changes due to physical channel changes can be measured by reciprocity using the downlink information; thus no feedback is required). Specifically, we find that the phase reciprocity expressed by (1) and (2) allows the relay to

feedback the phases of only two subcarriers to each end node, while ensuring the end node can recover the phases of all subcarriers. We will elaborate on how to achieve it in Section 3.5. Let us first introduce our solutions to the challenges 1) to 3) in Sections 3.3 and 3.4.

3.3 Channel Estimation and CFO Estimation

We address challenges 1) and 2) with fast CSI feedback and accurate CFO precoding. Our implementation of lattice-coded PNC is based on OFDM. As shown in Fig. 8, we adopt a packet format similar to that of 802.11, but with slight modifications. The preambles consist of STS and LTS. STS is a short training sequence of 16 samples; LTS is a long training sequence of 80 samples (including the 16 samples of CP). Only the DATA of the packets of nodes A and B overlap. Their STS and LTS do not overlap. We use the STS to detect packets, and the LTS before DATA to identify the starting position of the packet.

802.11	10 STS		2 LTS		DATA		
PNC A:	10 STS	0	LTS	0	DATA	LTS	0
PNC B:	0	10 STS	0	LTS	DATA	0	LTS

Fig. 8. Packet format.

Our channel-precoded PNC system places one LTS in the preamble and one LTS in the postamble for two reasons: 1) to obtain more up-to-date channel estimation based on the postamble, and 2) to obtain much more accurate CFO estimation by correlating the preamble LTS and the postamble LTS.

Specifically, channel estimation with preambles at the relay will induce a feedback delay equal to one PNC cycle, which consists of one uplink packet, one downlink packet, and the guard intervals in between packets. For lengthy packets, the feedback delay will then be long. Estimating the channel based on the postamble incurs a shorter feedback delay, and provides more up-to-date channel state information for the precoding of the next uplink packet.

More importantly, the packet format with preamble and postamble enables highly accurate CFO estimation, so that precoding can cancel out the CFO phase drift more completely. The IEEE 802.11 systems typically estimate CFO by correlating two consecutive LTS:

$$\text{CFO} = \frac{1}{\Delta N} \text{angle} \left(\sum_{i=0}^{63} lts_1^\dagger[i] \cdot lts_2[i] \right) \quad (3)$$

where lts_1 and lts_2 are the received signal of the two preamble LTS, ΔN is the separation between lts_1 and lts_2 , which is equal to 64 samples in 802.11. The correlation angle $\left(\sum_{i=0}^{63} lts_1^\dagger[i] \cdot lts_2[i]\right)$ finds the angle shift from lts_1 to lts_2 , and the division by their separation ΔN yields the CFO in the unit of radian/sample.

The noise embedded in lts_1 and lts_2 will induce CFO estimation errors. In our system, because the preamble and the postamble are separated by the data, ΔN can be more than 8,000 samples, much larger than the 64-sample separation of two LTS in the 802.11 preamble. This means that the noise will be averaged over a correlation interval that is more than 100 times longer than that of 802.11, yielding a CFO estimation 100 times more accurate than that of 802.11. Fig. 9 shows CFO estimation error (in log scale) versus ΔN under different SNR. We can see that the CFO estimation error for $\Delta N = 8,000$ is as small as $1/100$ of the CFO estimation error for $\Delta N = 64$.

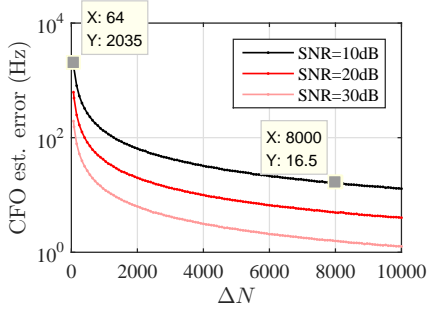


Fig. 9. CFO estimation error versus ΔN .

Another idea to remove the effect of noise on CFO estimation is to average the CFO estimates over multiple packets. However, this method has the side effect of smoothing out fast CFO variations of commercial TCXO, i.e., it does not react to CFO changes quickly. Fig. 10 shows the CFO estimation results with our preambles-postamble method in two seconds. The average CFO is about $7kHz$, but the variation can be larger than $0.4kHz$ within $100ms$. If we use the conventional 802.11 CFO estimation method and average the estimate over $100ms$ to remove noise, then the CFO estimation error can be hundreds of hertz, translating to a phase precoding error of more than $\pi/2$ radians in $1ms$. Therefore, the conventional 802.11 CFO estimation method does not work for the phase precoding in PNC.

Our preamble-postamble estimation method achieves high CFO estimation accuracy with an estimation interval (separation between the preamble

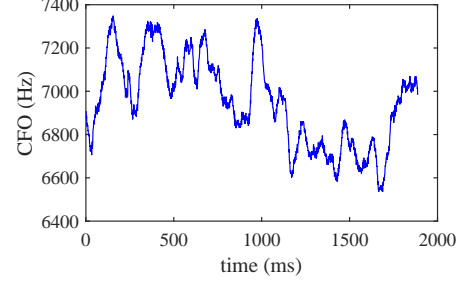


Fig. 10. CFO variation.

and the postamble) of about $0.5ms$, and a feedback delay (the separation between the postamble and the next packet) of about $0.5ms$. With the timely CFO estimates, the end nodes can precode CFO very accurately. When testing the overall phase alignment in our system (Figs. 3 and 4), we found that smoothing CFO estimates over multiple packets did not yield any improvement when TCXO is used. Instead, smoothing over more than 10 packets increased the phase error drastically, because the CFO coherence time is less than several milliseconds. Therefore, our reported experiments in Section 5 just used the estimates of the CFOs and channels from the most recent packet, without smoothing.

For simplicity of channel estimation, channel precoding and CFO precoding are performed on DATA part only, excluding the preambles and postambles. As a result, the phase drift from the preambles to the postambles can be more than one rotation as they are not CFO precoded. Meanwhile, the LTS correlation can only find the fractional rotation. In practice, we first estimate a rough CFO in the initialization phase. During the PNC experiments, we recover the full rotations based on the rough CFO and the fractional rotation, and then find the CFO.

3.4 Time Slot Synchronization

We address challenge 3) with tight synchronization in a time-slotted system. We built a time-slotted system to ensure two adjacent uplink packets will not have *uncontrollable* changes in the alignment of packet boundaries from time slot to time slot. In the time-slotted system, nodes A and B can only transmit at the beginnings of time slots. The number of samples separating two adjacent time slots is the same for nodes A and B. Thus, if the clocks of nodes A and B were exactly synchronized, the alignment of their packets at the relay would remain the same from time slot to time slot.

Due to the use of independent oscillators at nodes A and B, their time slots may be misaligned after a while even if they were synchronized in the beginning and that the same number of samples separate two adjacent time slots in both nodes. Thus, each end node will need to adjust its time slot boundaries once in a while to ensure time slot alignment (by momentarily adds or subtracts a few sample times from a time slot). A main difference of this mechanism with respect to the beacon-triggered mechanism is that the end nodes here know when they perform the adjustment and can compensate for the effect of the adjustment by modifying the phase of the channel precoding factor whenever it performs the time-slot adjustment (delay/advance is translated to phase change in the frequency domain at the OFDM receiver of the relay). In this way, the arrival-time jitters, which also happen in our system when an end node adjusts its time-slot boundary, can be “accounted for” and their effects can be compensated away through channel precoding. The next paragraph further elaborates this process.

Note that to achieve accurate phase alignment, we do not need highly accurate alignment of the arrival times of nodes A and B. We only need to keep track of the sample shifts across adjacent time slots accurately. With our time-slotted system, the sample shifts across adjacent time slots are caused by time-slot boundary adjustment, SFO, and sampling phase noise. The end node knows the time-slot boundary adjustment exactly and compensate for the phase change induced by the adjustment. Meanwhile, SFO and sampling phase noise cause only small sub-sample shifts across adjacent time slots. SFO can be estimated accurately and compensated for by SFO precoding, and sampling phase noise has very small effects according to our experiments with TCXO. Therefore, we can align the phases without very accurate timing synchronization, such as sub-nanosecond synchronization achieved by complicated hardware design [33]. Also note that even an error of 0.4 nanoseconds can result in phase change of $0.4ns \times 2.5GHz = 1$ rotation. Therefore, accurate timing synchronization is neither necessary nor sufficient for accurate phase alignment.

In the initialization phase of a PNC session, the relay sends a beacon to the end nodes to request them to start a timer. The timer defines time slots with fixed interval T_{slot} , and all nodes transmit packets according to the time slots defined by their timer. At the beginning of each time slot, each end node transmits an uplink packet. After receiving the

overlapped packets, the relay decodes the combined messages, estimates the channels of the end nodes, and then feedbacks the CSI to the end nodes. Since each end node maintains its own timer, there can be sample asynchrony between A and B. However, the sample asynchrony remains largely the same across adjacent time slots. The constant sample asynchrony ensures that the estimated channel in time slot 1 will still be valid for the precoding of the uplink packet in time slot 2.

In the long run, the SFO between the end nodes will accumulate and may cause the time slot boundaries to be offset by several samples. In our system, the relay monitors the time slot boundaries of the end nodes by correlating the received signal with the known LTS. The correlation will find 4 peaks: in the preamble, the first correlation peak indicates the end of the LTS of end node A, and the second peak indicates the end of the LTS of end node B; likewise for the postamble. Once the relay observes that the sample asynchrony grows larger than a threshold d_{thresh} (2 samples in our experiment), it will request the lagging end node to adjust its timer ahead by d_{thresh} samples to catch up with the other node. This sample adjustment will change the frequency-domain channel. Thus, an end node needs to adjust the frequency-domain precoding coefficients each time it adjusts the time slot boundary. To cancel the effect of advancing by d_{thresh} samples, the end node multiplies the k -th subcarrier by

$$e^{-j \cdot 2\pi k d_{\text{thresh}} / 64}. \quad (4)$$

This multiplication mimics delaying d_{thresh} samples in the time domain. In this way, we align slot boundaries while ensuring the channel precoding is still valid.

3.5 Reciprocity-Based Phase Precoding

As discussed in Section 3.2, channel reciprocity cannot enable phase precoding without any feedback. In this subsection, we explain how to exploit channel reciprocity to minimize the amount of phase feedback information required.

We start by subtracting (1) by (2) to get

$$\theta_{\text{up}}(t_2) = \theta_{\text{up}}(t_1) - \theta_{\text{dn}}(t_1) + \theta_{\text{dn}}(t_2) + 2\eta(t_1, t_2). \quad (5)$$

The term $\eta(t_1, t_2)$ consists of the phase changes caused by CFO phase drift, SFO sample drift, carrier phase noise, and sampling phase noise. The phase change caused by CFO phase drift and carrier phase noise is common across all subcarriers. The phase

TABLE 1
Comparisons with other precoding systems.

	Extra Antennas	Extra band	Extra node	Shared clock	Non-commercial oscillator	Feedback overhead	95 th percentile misalignment (rad)	95 th percentile misalignment deviation (rad)
This paper	✗	✗	✗	✗	✗	4% of full feedback	0.18 (partial feedback), 0.15 (full feedback)	0.10 (partial feedback), 0.08 (full feedback)
AirSync [13]	✓	✓	✓	✗	✗	full	0.08	
JMB [12]	✗	✗	✓	✗	✓	full		0.05
Argos [12]	✗	✗	✗	✓	✗	N/A		

change caused by SFO sample drift and sampling phase noise is linear in the shifted subcarrier index

$$k' = \begin{cases} k, & k < \frac{N}{2} \\ k - N, & k \geq \frac{N}{2} \end{cases}. \quad (6)$$

Note that using the shifted subcarrier index, $k' = 0$ corresponds to the DC subcarrier, $k' > 0$ corresponds to a subcarrier with positive frequency, and $k' < 0$ corresponds to a subcarrier with negative frequency. Thus, the overall $\eta(t_1, t_2)$ is linear in k' , i.e.

$$\eta(t_1, t_2) = c_0 + c_1 k' \quad (7)$$

where $c_0, c_1 \in \mathbb{R}$ are linear coefficients. It can be expanded as

$$\eta(t_1, t_2) = 2\pi \int_{t_1}^{t_2} \left[\text{CFO}(\tau) + \text{SFO}(\tau) \cdot \frac{k'}{N} \right] d\tau \quad (8)$$

if we ignore phase noise. In (8), the CFO term $2\pi \int_{t_1}^{t_2} \text{CFO}(\tau) d\tau$ is due to the cumulative phase drift caused by CFO over time. All subcarriers suffer the same phase drift due to CFO (note: before doing phase estimation using the OFDM symbol in the LTS, the receiver needs to compensate for this CFO phase drift on the OFDM symbol). The SFO induces fractional sample shifts which translate to different phase shifts in different subcarriers. In FFT, shifting integer samples Δd causes phase rotation of $2\pi \Delta d \frac{k}{N}$, or equivalently $2\pi \Delta d \frac{k'}{N}$ with k' as the shifted index of k . Although both the expressions with k and k' are valid for integer-sample shifts, when the shifting theorem extends to fractional-sample shifts, the phase rotation must be expressed as proportional to the shifted index k' . As the fractional-sample shift is $\int_{t_1}^{t_2} \text{SFO}(\tau) d\tau$, the SFO term will be $2\pi \int_{t_1}^{t_2} \text{SFO}(\tau) \cdot \frac{k'}{N} d\tau$.

The linearity of $\eta(t_1, t_2)$ suggests that the phases of any two subcarriers k_1 and k_2 should be sufficient for an end node to recover the phases of all 52 subcarriers. Adding a superscript k to $\theta_{\text{up}}(t)$, we use

$\theta_{\text{up}}^k(t)$ to denote the uplink phase at subcarrier k , and similarly for $\eta^k(t_1, t_2)$. From the two feedback phases $\theta_{\text{up}}^{k_1}(t_2)$ and $\theta_{\text{up}}^{k_2}(t_2)$, the end node can find the corresponding $\eta^{k_1}(t_1, t_2)$ and $\eta^{k_2}(t_1, t_2)$, then interpolate to find $\eta^k(t_1, t_2)$ for all k , and finally find $\theta_{\text{up}}^k(t_2)$ for all k . The phase precoding error does not grow with time, because in each time slot the feedback phases of two subcarriers can reset the phase error caused by estimation error of CFO and SFO.

To make the interpolation (linear regression) more robust against noise, we feedback the phases of the subcarriers with shifted index $k'_1 = -26$ and $k'_2 = 26$. Two subcarriers separated this far, however, may suffer from the 2π wrap-around problem that can invalidate the phase interpolation. We resolve the 2π wrapping ambiguity by matching the interpolated phases to phases predicted by adding CFO and SFO phase drifts to the phases of the previous time slot. In addition to the above, the variation of the channel estimation times (CP cut positions of the received LTS) across successive packets and the integer-sample adjustment of time slot boundary, if not taken care of, will also mess up the phase precoding. We need to keep track of these integer sample changes in the downlink and the uplink to compensate for the accumulated integer sample differences from the initial calibration.

Note that the above analysis is simplified by assuming the uplink phase and downlink phase can be estimated at the same time. The analysis is still valid when we consider the practical case in which the phases are estimated at different times. Just that we need to use CFO and SFO estimates to compensate for extra phase drift in the mismatched estimation times. This causes only limited phase error due to estimation errors of the CFO and the SFO.

Finally, with the uplink phase $\theta_{\text{up}}^k(t_2)$, CFO, and SFO, an end node should precode its phases of the next uplink packet with additive phase offsets. At

time t_3 when transmitting the next uplink packet, as in (8), the phase change from t_2 to t_3 is $\eta^k(t_2, t_3) = 2\pi \int_{t_2}^{t_3} [\text{CFO}(\tau) + \text{SFO}(\tau) \cdot \frac{k'}{N}] d\tau$, and thus the uplink phase at time t_3 will be $\theta_{\text{up}}^k(t_2) + \eta^k(t_2, t_3)$. To compensate for this phase change, the end node should precode its phase at time t_3 by precoding with

$$-\theta_{\text{up}}^k(t_2) - 2\pi \cdot \left[\text{CFO} + \text{SFO} \cdot \frac{k'}{N} \right] \cdot [t_3 - t_2] \quad (9)$$

for subcarrier k . Note that t_3 changes within the packet. The overall error of this phase precoding process consists of the error in $\theta_{\text{up}}^k(t_2)$, the estimation errors of CFO and SFO, and the channel changes from t_2 to t_3 .

Using our reciprocity-based phase precoding scheme, the relay feedbacks the phases of all subcarriers only once during the initial calibration. After that, the relay only feedbacks the phases of two subcarriers to each end node in each time slot. In each time slot, for each end node, the relay only needs to feedback 4 coefficients: 2 coefficients for the phases of two subcarriers, 1 for amplitude, and 1 for CFO. In long run, the amount of amplitude feedback information is cut by $(52 - 1)/52 \approx 98\%$, and the amount of phase feedback information is cut by $(52 - 2)/52 \approx 96\%$. We use a 4-byte floating point number to represent each coefficient; so the feedback data is 16 bytes altogether. As our packet payload length is more than 1,500 bytes, the feedback data amount is as little as 1%. Note that we could further reduce the amount of feedback by quantizing a feedback coefficient with fewer bits. For the phases and amplitudes, quantization errors of $1/1000$ are sufficient to ensure negligible penalty to the precoding. So using 10 bits to represent a coefficient will be good enough.

3.6 Comparisons with Other Precoding Systems

Tab. 1 compares the resource consumptions, communication overheads, and phase alignment performances of our precoding system with those of prior work. Each of these prior precoding systems requires the use of at least one of the following: (i) extra antennas; (ii) extra band; (iii) extra node; (iv) shared clock, or (v) non-commercial oscillator. Our system does not require any of the above and is amenable to simple practical deployment. Moreover, our overall feedback overhead is just $\frac{4}{52 \times 2 + 1} \approx 4\%$ of full feedback. AirSync [13] and JMB [12] did not incorporate any methods to reduce the feedback

overhead. The precoding scheme in Argos [29] is not applicable to TWRN with distributed nodes; the overhead cannot be meaningfully compared and therefore omitted in the table. Some entries are missing in the last two columns because they are not provided in the corresponding papers. As a price for practicality, our system does incur larger phase misalignment compared with [12], [13]. Fortunately, the residual phase misalignment (shown in Figs. 3 and 4) can be handled by our lattice decoder design which will be described in the next section.

4 LDLC ENCODING AND DECODING

This section presents the LDLC encoding and decoding methods in our lattice-coded PNC system. Our LDLC design is built upon that in [17], [20], with improvement and customization on the lattice shaping and decoding to suit our PNC implementation.

4.1 LDLC Encoding

A general coding lattice can be defined by a generating matrix $\mathbf{G} \in \mathbb{C}^{n \times m}$, where $n \geq m$, with a corresponding parity check matrix $\mathbf{H} = \mathbf{G}^{-1} \in \mathbb{C}^{m \times n}$ (\mathbf{G}^{-1} is the pseudo inverse of \mathbf{G} if $m \neq n$). A lattice code can be defined by a coding lattice and a shaping region to control the power of the codewords. LDLC is a special class of lattice codes with a sparse parity check matrix \mathbf{H} . Each row and each column of \mathbf{H} has at most d non-zeros elements. The non-zero elements are generated from a generating sequence $\mathbf{h} = [h_1, \dots, h_d]$; see [15], [17] for details on how to generate \mathbf{h} and \mathbf{H} . The sparsity of \mathbf{H} allows BP decoding in linear complexity.

We encode by

$$\mathbf{t} = \mathbf{G}\mathbf{b} \quad (10)$$

where $\mathbf{b} \in \mathbb{Z}^m[i]$ is a Gaussian integer vector representing the message, and $\mathbf{t} \in \mathbb{C}^n$ is the encoded lattice codeword. The encoding in (10) has complexity $O(m \cdot n)$, but can be simplified by solving the sparse equation $\mathbf{H}\mathbf{t} = \mathbf{b}$ to find \mathbf{t} . We constrain each element b_i in \mathbf{b} to be a member of the Gaussian integer alphabet

$$\mathcal{B} = \{b_{i,I} + jb_{i,Q}, b_{i,Q} \in \mathcal{A}\} \quad (11)$$

where $\mathcal{A} = \{a \in \mathbb{Z} | a_l \leq a \leq a_u, \text{ where } a_l, a_u \in \mathbb{Z} \text{ with } a_l \leq a_u\}$ is an integer alphabet.

Among all possible codewords, some codewords may have very large power. If we just transmit \mathbf{t} , we will have to use a very small gain at the RF front end (both transmitter and receiver) to

avoid saturating the amplifier. Generally, we need lattice shaping to control the power of the lattice codeword.

4.2 Fixed-Complexity Hypercube Shaping

For a given message \mathbf{b} , the goal of shaping is to map \mathbf{b} to $\tilde{\mathbf{b}}$ so that the resulting codeword $\tilde{\mathbf{t}} = \mathbf{G}\tilde{\mathbf{b}}$ has small power. By choosing a $\tilde{\mathbf{b}}$ such that $\tilde{\mathbf{b}} \equiv \mathbf{b}$ up to a modulo operation, the receiver can obtain the original message \mathbf{b} by taking modulo after decoding $\tilde{\mathbf{b}}$ from $\tilde{\mathbf{t}}$.

We adopt hypercube shaping [16] in this paper. Hypercube shaping performs shaping on \mathbf{t} and \mathbf{b} element-wise with the power of each element of $\tilde{\mathbf{t}}$ being individually constrained. Specifically, we do RQ decomposition $\mathbf{H} = \mathbf{R}\mathbf{Q}$, where $\mathbf{R} \in \mathbb{C}^{m \times n}$ is a lower-triangular matrix, and $\mathbf{Q} \in \mathbb{C}^{n \times n}$ is a unitary matrix. Then from $\mathbf{H}\mathbf{t} = \mathbf{b}$, we have $\mathbf{R}\mathbf{Q}\mathbf{t} = \mathbf{R}\mathbf{t}' = \mathbf{b}$. Correspondingly, we have $\mathbf{R}\mathbf{Q}\tilde{\mathbf{t}} = \mathbf{R}\tilde{\mathbf{t}}' = \tilde{\mathbf{b}}$. Then we perform shaping on \mathbf{t}' (i.e. obtain $\tilde{\mathbf{t}}'$) by mapping b_i to \tilde{b}_i from $i = 1$ to $i = m$ in a one-by-one manner. We can determine $\tilde{b}_i, i = 1, \dots, m$ successively thanks to the fact that \mathbf{R} is lower-triangular. Starting with $i = 1$, for each successive b_i , we find $\tilde{b}_i \equiv b_i$ such that the corresponding \tilde{t}'_i has the lowest power. The powers of $\tilde{\mathbf{t}}' = \mathbf{Q}\tilde{\mathbf{t}}$ and $\tilde{\mathbf{t}}$ are equal because \mathbf{Q} is a unitary matrix. After the shaping process, the transmitter transmits $\tilde{\mathbf{t}}$.

As a result of the hypercube shaping, the elements in $\tilde{\mathbf{b}}$ are no longer constrained in the alphabet \mathcal{B} . Rather, the Gaussian integer alphabet of the shaped message $\tilde{\mathbf{b}}$ is

$$\tilde{\mathcal{B}} = \left\{ \tilde{b}_{i,I} + j\tilde{b}_{i,Q} | \tilde{b}_{i,I}, \tilde{b}_{i,Q} \in \tilde{\mathcal{A}} \right\}. \quad (12)$$

where $\tilde{\mathcal{A}} \subset \mathbb{Z}$ is the integer alphabet after shaping. The conventional hypercube shaping does not limit the size of $\tilde{\mathcal{A}}$. However, the computation complexities of the shaping and the BP decoding [17] with respect to $|\tilde{\mathcal{A}}|$ are $O(|\tilde{\mathcal{A}}|^2)$. The nonlinear complexity will increase the complexity of BP decoding dramatically if $|\tilde{\mathcal{A}}|$ is large. Fortunately, we find that the probability of the shaped elements $\tilde{b}_{i,I}$ or $\tilde{b}_{i,Q}$ straying far away from the origin is very low in general. Therefore, for our implementation, we use a fixed-complexity hypercube shaping algorithm that limits $\tilde{\mathcal{A}}$ to

$$\tilde{\mathcal{A}} = \{ \tilde{a} \in \mathbb{Z} | \min(\mathcal{A}) - |\mathcal{A}| \leq \tilde{a} \leq \max(\mathcal{A}) + |\mathcal{A}| \} \quad (13)$$

i.e., the shaped integer alphabet $\tilde{\mathcal{A}}$ is triple the size of \mathcal{A} , also centered around the origin. Limiting the range of $\tilde{\mathcal{A}}$ as such will cause the power of the

resulting codeword to be larger than ideal shaping without limits. To examine the penalty incurred, we did a Monte-Carlo simulation to find the probability distribution of the shaped elements \tilde{b}_i , where we expanded $\tilde{\mathcal{A}}$ to $\tilde{\mathcal{A}}' = \{ \tilde{a} \in \mathbb{Z} | \min(\mathcal{A}) - 2|\mathcal{A}| \leq \tilde{a} \leq \max(\mathcal{A}) + 2|\mathcal{A}| \}$, with $\mathcal{A} = \{-1, 0, 1\}$. The probability distribution of \tilde{b}_i from these simulations based on $\tilde{\mathcal{A}}'$ are shown in Fig. 11. We observed that the probability of $\tilde{b}_{i,I}$ or $\tilde{b}_{i,Q}$ falling outside of the $\tilde{\mathcal{A}}$ in (13) is in the ballpark of 10^{-6} . This implies that our fixed-complexity hypercube shaping based on $\tilde{\mathcal{A}}$ in (13) will not have much penalty.

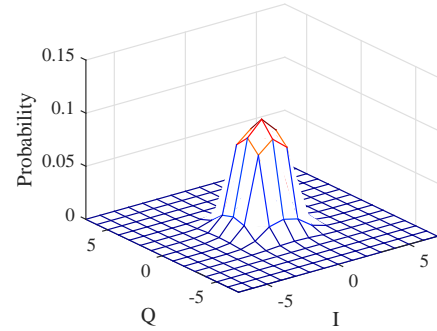


Fig. 11. Probability distribution of the shaped Gaussian integer alphabet, where $\mathcal{A} = \{-1, 0, 1\}$.

In the following, we first introduce the LDLC decoding for point-to-point channel, and then extend the point-to-point decoder to our PNC decoder.

4.3 LDLC Decoding in Single-user Systems

After the LDLC encoding, we place the elements of the codeword $\tilde{\mathbf{t}}$ on the OFDM subcarriers, and then do Inverse Fast Fourier Transform (IFFT) to convert the frequency-domain signal to time-domain signal $\mathbf{x} \in \mathbb{C}^n$ before transmission. The receiver transforms the signal back to the frequency domain. The frequency-domain model can be written as $\mathbf{y} = \tilde{\mathbf{t}} + \mathbf{w}$ where $\mathbf{y} \in \mathbb{C}^n$ is the signal after channel compensation, and $\mathbf{w} \in \mathbb{C}^n$ is a noise term. The BP decoder passes messages between the check nodes and variable codes iteratively to decode for $\tilde{\mathbf{b}}$. Specifically, the BP decoder checks

$$\mathbf{H}\tilde{\mathbf{t}} = \tilde{\mathbf{b}} \in \tilde{\mathcal{B}}^m. \quad (14)$$

An individual check node i has a check equation given by $\sum_k h_{ik}\tilde{t}_k = \tilde{b}_i \in \tilde{\mathcal{B}}$, where k traverses the indices of the non-zero elements of the i -th row of \mathbf{H} .

4.4 LDLC Decoding in PNC

This subsection extends the LDLC decoder to decode a linear combination of the messages of two

end nodes for the purpose of PNC. The prior theoretical works on lattice decoding in PNC and CF [21], [27] proposed to decode an integer combination of the messages in the presence of channel misalignment. Computing integer combination requires multiplying the received signal by a scaling factor to match the integer coefficients. The scaling operation will amplify noise and thus degrade the decoding performance. If the phase misalignment is severe and the scaling factor is large, then this scaling-computing scheme only works under high signal-to-noise ratio (SNR). To achieve the best decoding performance and avoid wasting power, it is desirable to minimize the channel misalignment such that we can choose the scaling factor to be small. Luckily, the phase alignment mechanism in the preceding sections can fulfill this need, so that our system can work well with moderate SNR.

The prior works [21], [27] assumed constant random channel misalignments between users throughout a packet. The practical case in our system is different: the phase misalignment is small, but it varies throughout a packet. We can keep track of the phase with the pilots in OFDM symbols (each end node has two pilots and the pilots from different end nodes do not overlap). Since we have precoded the channel and made the misalignment nearly zero, the difference between different subcarriers are nearly zero. The phases of different subcarriers may shift in the same direction due to residual CFO caused by CFO estimation error. Therefore, for each end node, the relay can find the average phase of its two pilots in an OFDM symbol to estimate the phases of all subcarriers.

In the remainder of this subsection, we introduce our LDLC decoder that takes into account the per-symbol phase misalignments. We aim to compute $\tilde{\mathbf{t}}_A + \tilde{\mathbf{t}}_B$. The frequency-domain PNC channel model of our system is

$$\mathbf{y} = \tilde{\mathbf{t}}_A + \mathbf{P}\tilde{\mathbf{t}}_B + \mathbf{w} = \tilde{\mathbf{t}}_P + \mathbf{w} \quad (15)$$

where $\tilde{\mathbf{t}}_A \in \mathbb{C}^n$ and $\tilde{\mathbf{t}}_B \in \mathbb{C}^n$ are the lattice codewords from end nodes A and B respectively, $\tilde{\mathbf{t}}_P = \tilde{\mathbf{t}}_A + \mathbf{P}\tilde{\mathbf{t}}_B$ is the received combination of $\tilde{\mathbf{t}}_A$ and $\tilde{\mathbf{t}}_B$, and $\mathbf{P} = \text{diag}(p_1, \dots, p_n)$ represents the phase offset between $\tilde{\mathbf{t}}_A$ and $\tilde{\mathbf{t}}_B$, with p_j representing the channel misalignment (in both amplitude and phase) in the j -th dimension (estimated with the pilots). Note that we have normalized the channel of A to be one. In general, p_1, \dots, p_n are different. We scale \mathbf{y} element by element separately with β_1, \dots, β_n to obtain $\tilde{y}_j = \beta_j y_j$. In a matrix form, we

have $\tilde{\mathbf{y}} = \mathbf{B}\mathbf{y}$ where $\mathbf{B} = \text{diag}(\beta_1, \dots, \beta_n)$. The goal of the scaling is to match

$$\tilde{y}_j = \beta_j \tilde{t}_{A,j} + \beta_j p_j \tilde{t}_{B,j} + \beta_j w_j \quad (16)$$

to $\tilde{t}_{A,j} + \tilde{t}_{B,j}$ better. By minimal mean square error (MMSE) rule, we have

$$\beta_j = \frac{1 + p_j^\dagger}{\sigma^2 + 1 + |p_j|^2} \quad (17)$$

where σ^2 is the noise variance. After the scaling operation, we use the LDLC decoder in the last subsection to decode $\tilde{\mathbf{b}}_A + \tilde{\mathbf{b}}_B$. Finally, we calculate

$$\mathbf{b}_{\text{PNC}} = (\tilde{\mathbf{b}}_A + \tilde{\mathbf{b}}_B) \bmod \mathcal{A} = (\mathbf{b}_A + \mathbf{b}_B) \bmod \mathcal{A}. \quad (18)$$

The relay then sends \mathbf{b}_{PNC} to the two end nodes. Each end node can recover the message from the other end node by subtracting its own message from \mathbf{b}_{PNC} and then taking modulo on \mathcal{A} .

The Effect of Shaping on Decoding: The conventional LDLC decoders [15], [17], [27] assumed equiprobable alphabet, and extended the check node messages with respect to all elements in the alphabet in the same way in the BP iterations. However, Fig. 11 shows that the hypercube shaping yields an alphabet with Gaussian-like probability distribution, and thus the probability distribution of the checksum is also Gaussian-like. We also take into account this more accurate probability distribution in our decoder. In the message passing between the check nodes and variable nodes in the BP iterations, we scale the information from a checksum $(\tilde{b}_{A,j} + \tilde{b}_{B,j})$ with a weight proportional to its probability.

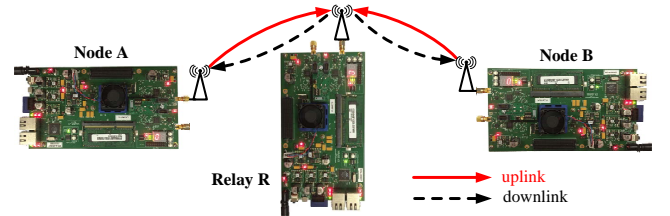


Fig. 12. PNC on WARP.

5 EXPERIMENTS

This section presents our implementations and experimental results. Fig. 12 shows our SDR implementation of PNC on the wireless open access research platform (WARP) [34]. In our experimental set-up, three WARP nodes serve as the relay, node A, and node B. The nodes are placed in an indoor office environment, with pairwise separation ranging from 2 meters to more than 10 meters.

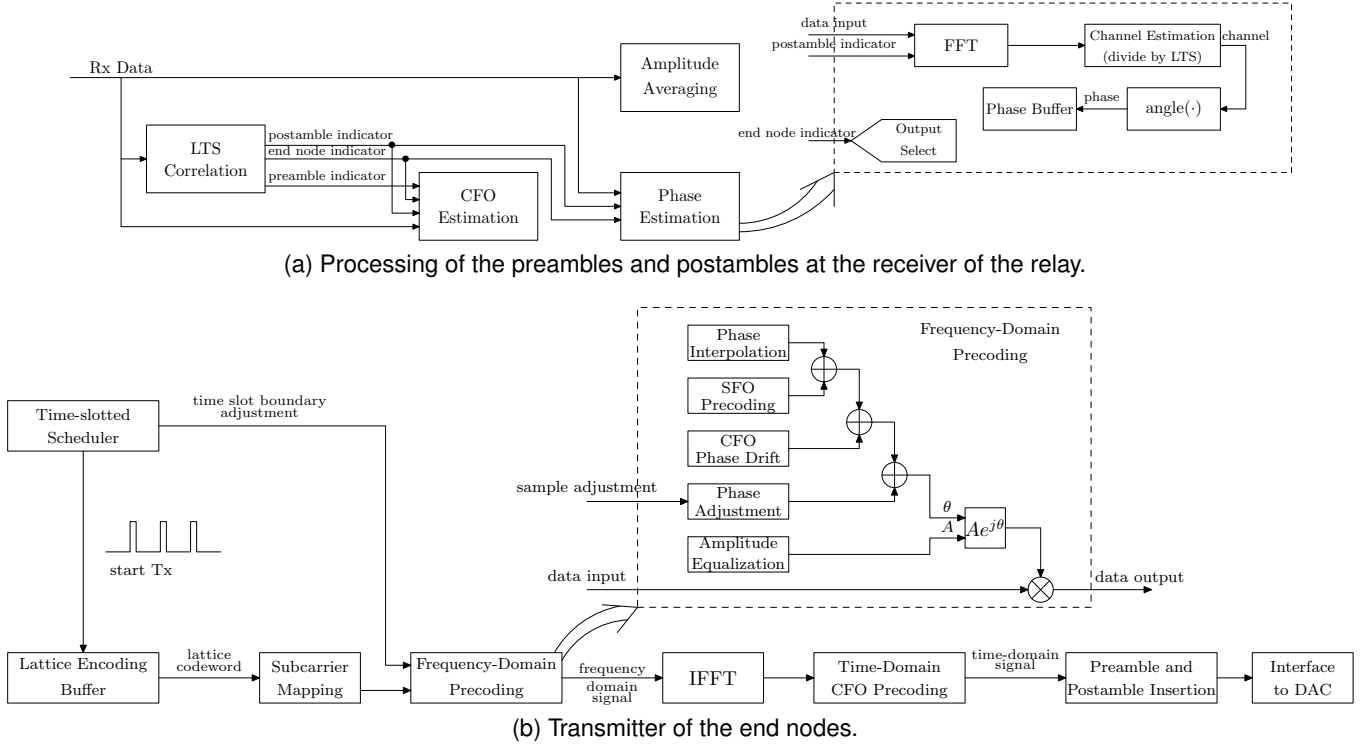


Fig. 13. System Diagrams.

In what follows, we put together all the functionalities described in the preceding sections for an overall design, and describe the FPGA implementation of time-critical functions that achieves an effective feedback delay (from channel estimation to using the channel estimate for precoding) of about $0.5ms$. Then we present our experiment results. The measurements of our phase precoding has already been shown in Figs. 3 and 4. To demonstrate the advantage of PNC over traditional methods and justify the motivation of PNC, in this section we compare the BER of TD, SNC, and PNC in two-user relay networks. Finally, we present the throughputs of lattice-coded PNC with different coding rate, in both static LoS scenario and mobile non-LoS scenario.

5.1 FPGA Implementations

Fig. 13 shows the block diagrams of the FPGA receiver design of the relay and the transmitter design of the end nodes, based on WARP 802.11 reference design. The receiver of the end nodes and the transmitter of the relay follow the standard of the OFDM PHY layer of 802.11, but without the MAC layer of 802.11.

In the receiver diagram of the relay, the LTS correlation block determines the sample positions of the preambles and postambles in the received data,

and indicates whether the preamble or postamble currently under processing belongs to node A or B. The CFO estimation block estimates the CFO of each node based on (3) and the rough CFO. The channel estimation block estimates the frequency-domain (subcarrier) channels of each end node based on the received postamble. The amplitude averaging block averages the amplitudes of pilots to get an overall amplitude scaler for feedback to the end node. All the above processing can be completed within $10\mu s$ after the reception of the postamble.

In the transmitter diagram of the end nodes, the time-slotted scheduler schedules packet transmissions according to the timer that was set in the initialization phase. It also adjusts the timer occasionally (when requested by the relay) to align slot boundaries. Each packet contains five lattice codewords. The lattice codewords are first mapped to the OFDM subcarriers. Then the frequency-domain precoding block precodes both the phase and amplitude for different subcarriers. In the frequency-domain precoding block, the phase interpolation block recovers the phase of each subcarrier by interpolating with the partial feedback of phases. The CFO phase drift block calculates the phase drift due to the CFO from the time when the postambles of last packet was transmitted to the time when the data part of the current packet will be transmitted. The SFO precoding block calculates the SFO phase

shift from the time when the postamble of last packet was transmitted to the time when the current OFDM symbol of the current packet will be transmitted. The phase adjustment block implements (4). The amplitude equalization block calculates the absolute amplitude precode factors for the uplink subcarriers based on the relative downlink amplitudes of the subcarriers and the feedback amplitude scaler. The amplitude precode factor and the phase of each subcarrier then forms a complex precode factor for the subcarrier that will be multiplied to the frequency-domain signal before transmission. After that, the time-domain CFO precoding block compensates for the phase drift in the data part. All the above precoding processing can be completed within $10\mu s$ after the reception of the downlink packet from the relay. That is, the transmission of the next uplink packet can be started within $10\mu s$ of the reception of the downlink packet.

5.2 BER of TD, SNC, and PNC

To compare TD, SNC, and PNC fairly, we did an experiment to measure the BER of the three schemes for the same normalized end-to-end data delivery rate with QAM modulation without channel coding. As TD, SNC, and PNC take 4, 3, and 2 non-overlapping transmissions respectively, we use 256-QAM (8 bits/symbol) for TD, 64-QAM (6 bits/symbol) for SNC, and 16-QAM (4 bits/symbol) for PNC, such that they have the same normalized end-to-end data delivery rate of $\frac{8}{4} = \frac{6}{3} = \frac{4}{2} = 2$ bits/symbol. We do not incorporate channel coding so as to have a clean comparison of the transmission schemes.

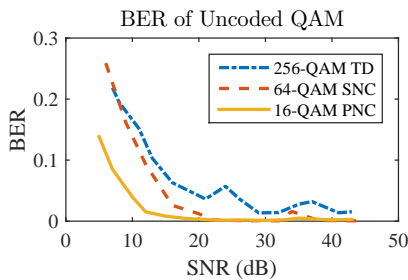


Fig. 14. BER of uncoded TD, SNC, and PNC for the same normalized end-to-end data delivery rate.

The experiment results in Fig. 14 demonstrate that PNC can achieve lower BER for the same normalized data delivery rate, especially at low-SNR regime. This is because PNC can afford to use the lower-order modulation for the same data delivery rate.

5.3 Throughput Performance of Lattice-Coded PNC

We now present the throughput performance of the overall lattice-coded PNC system in static LoS scenario and mobile non-LoS scenario. Each LDLC codeword of $n = 960$ symbols is mapped to $N_s = 20$ OFDM symbols, each consisting of the 48 data-carrying OFDM subcarriers (i.e., the data subcarriers in 802.11). Each uplink packet contains $N_c = 5$ LDLC codewords, i.e. 100 OFDM symbols, the preamble, and the postamble. The time slot duration is $T_{\text{slot}} = 1ms$, with $0.5ms$ for uplink followed by $0.5ms$ for downlink. The source message associated with each LDLC codeword consists of m complex source symbols. The real and complex parts of each source symbol are elements of the integer alphabet $\mathcal{A} = \{-1, 0, 1\}$. Taking into account the overhead of the preamble and postamble, the silence period, and the downlink period, the maximum throughput (if all messages are delivered successfully) of each end node is $r_n = \frac{N_c \cdot m \cdot \log_2 9}{T_{\text{slot}}}$. In our experiments below, we evaluate the throughput using different code rates $\frac{m}{n}$ by setting $m = 800$ ($r_n = 12.7Mbps$) and $m = 900$ ($r_n = 14.3Mbps$). For the mobile non-LoS experiments, the end nodes were randomly placed at locations where the direct path to the relay was blocked by obstacles. Two persons held the two end nodes separately and walked at ordinary speed.

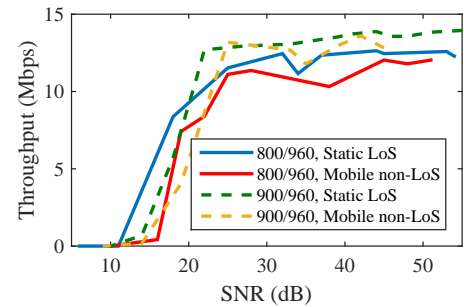


Fig. 15. Normalized PNC throughput with different code rates in static LoS and mobile non-LoS scenarios.

As shown in Fig. 15, our lattice-coded PNC system achieves good throughput performance using code rates 800/960 and 900/960 in the static LoS and the mobile non-LoS scenarios. In the low SNR regime, the mobile non-LoS scenario has a penalty of $2 \sim 4dB$ with respect to the static LoS scenario. In the high SNR regime, our system can approach the maximum throughput in the static LoS scenario and have a small gap from the maximum throughput in the mobile non-LoS scenario. The penalties in the

mobile non-LoS scenario are incurred by the channel variation due to motion and frequency selective fading (probably deep fading in some subcarriers). Fig. 15 also shows that code rate 900/960 yields higher throughput in the high SNR regime than that of code rate 800/960, while code rate 800/960 yields higher throughput in the low SNR regime since lower code rate can reduce packet error rate. We remark that without channel alignment, the throughputs in all the above cases will be practically zero.

6 CONCLUSION

This paper presented a first implementation of a practical lattice-coded PNC system. Our system achieves accurate channel alignment of distributed nodes using only temperature-compensated oscillators, without the need for extra antennas or bandwidth to broadcast reference signal. The accurate channel alignment is attributed to two critical components: 1) a CFO estimation method that is 100 times more accurate than the conventional 802.11 method; 2) fast CSI feedback in the ballpark of 0.5ms. Our channel precoding system also has very low signaling overhead and, by exploiting channel reciprocity, it requires partial CSI feedback that is only as little as 1% of the data payload. In addition to the tight channel alignment, we also redesigned the lattice encoding and decoding algorithms to deal with the challenges of encoding/decoding complexity and residual channel misalignments. We demonstrated good throughput performance of the implemented PNC system in static LoS and mobile non-LoS scenarios. Prior to our work here, investigations of lattice-coded communication systems (PNC or non-PNC) existed primarily in the theoretical domain. We believe our work is an important first step toward making lattice-coded communication systems practical.

REFERENCES

- [1] S. Zhang, S. C. Liew, and P. P. Lam, "Hot topic: physical-layer network coding," in *ACM MobiCom 2006*. ACM, 2006, pp. 358–365.
- [2] P. Popovski and H. Yomo, "The anti-packets can increase the achievable throughput of a wireless multi-hop network," in *ICC 2006*, vol. 9. IEEE, 2006, pp. 3885–3890.
- [3] S. Katti, H. Rahul, W. Hu, D. Katabi, M. Médard, and J. Crowcroft, "Xors in the air: practical wireless network coding," in *ACM SIGCOMM computer communication review*, vol. 36, no. 4. ACM, 2006, pp. 243–254.
- [4] L. Lu, L. You, and S. Liew, "Network-coded multiple access," *IEEE Trans. Mobile Comput.*, 2014.
- [5] L. You, S. C. Liew, and L. Lu, "Network-coded multiple access ii: Toward realtime operation with improved performance," *IEEE J. Sel. Areas Commun.*, vol. 33, no. 2, pp. 264–280, February 2015.
- [6] W. Nam, S.-Y. Chung, and Y. H. Lee, "Capacity of the Gaussian two-way relay channel to within 1/2 bit," *IEEE Trans. Inf. Theory*, vol. 56, no. 11, pp. 5488–5494, 2010.
- [7] Y. Chen, D. Haley, and Q. B. Nguyen, "Frequency offset compensation in physical-layer network coding systems," in *Communications Theory Workshop (AusCTW), 2013 Australian*. IEEE, 2013, pp. 146–151.
- [8] L. Lu, T. Wang, S. C. Liew, and S. Zhang, "Implementation of physical-layer network coding," *Physical Communication*, vol. 6, pp. 74–87, 2013.
- [9] A. C. Marcum, J. V. Krogmeier, D. J. Love, and A. Sprintson, "Analysis and implementation of asynchronous physical layer network coding," *IEEE Trans. Wireless Commun.*, vol. 14, no. 12, pp. 6595–6607, 2015.
- [10] X. Wang and W. Mao, "Analog network coding without restrictions on superimposed frames," *IEEE/ACM Trans. Netw.*, no. 99, 2015.
- [11] M. Wu, F. Ludwig, M. Woltering, D. Wübben, A. Dekorsy, and S. Paul, "Analysis and implementation for physical-layer network coding with carrier frequency offset," in *18th International ITG Workshop on Smart Antennas (WSA)*, 2014, pp. 1–8.
- [12] H. S. Rahul, S. Kumar, and D. Katabi, "Jmb: scaling wireless capacity with user demands," in *ACM SIGCOMM 2012*. ACM, 2012, pp. 235–246.
- [13] H. V. Balan, R. Rogalin, A. Michaloliakos, K. Psounis, and G. Caire, "Airsync: Enabling distributed multiuser mimo with full spatial multiplexing," *IEEE/ACM Trans. Netw.*, vol. 21, no. 6, pp. 1681–1695, 2013.
- [14] O. Abari, H. Rahul, D. Katabi, and M. Pant, "Airshare: Distributed coherent transmission made seamless," in *INFOCOM 2015*. IEEE, 2015, pp. 1742–1750.
- [15] N. Sommer, M. Feder, and O. Shalvi, "Low-density lattice codes," *IEEE Trans. Inf. Theory*, vol. 54, no. 4, pp. 1561–1585, 2008.
- [16] —, "Shaping methods for low-density lattice codes," in *ITW 2009*. IEEE, 2009, pp. 238–242.
- [17] Y. Yona and M. Feder, "Complex low density lattice codes," in *ISIT 2010*. IEEE, 2010.
- [18] S. C. Liew, S. Zhang, and L. Lu, "Physical-layer network coding: Tutorial, survey, and beyond," *Physical Communication*, vol. 6, pp. 4–42, 2013.
- [19] B. Hern and K. Narayanan, "Multilevel coding schemes for compute-and-forward with flexible decoding," *IEEE Trans. Inf. Theory*, vol. 59, no. 11, pp. 7613–7631, Nov. 2013.
- [20] U. Erez and R. Zamir, "Achieving $1/2\log(1+\text{SNR})$ on the AWGN channel with lattice encoding and decoding," *IEEE Trans. Inf. Theory*, vol. 50, no. 10, pp. 2293–2314, Oct. 2004.
- [21] B. Nazer and M. Gastpar, "Compute-and-forward: Harnessing interference through structured codes," *IEEE Trans. Inf. Theory*, vol. 57, no. 10, pp. 6463–6486, 2011.
- [22] U. Niesen and P. Whiting, "The degrees of freedom of compute-and-forward," *IEEE Trans. Inf. Theory*, vol. 58, no. 8, pp. 5214–5232, 2012.
- [23] A. Sakzad, E. Viterbo, J. Boutros, and Y. Hong, "Phase precoded compute-and-forward with partial feedback," in *ISIT 2014*. IEEE, 2014, pp. 2117–2121.
- [24] O. Ordentlich, U. Erez, and B. Nazer, "On compute-and-forward with feedback," in *ITW 2015*. IEEE, 2015, pp. 1–5.

- [25] D. Kramarev, A. Sakzad, and E. Viterbo, "Implementation of a two-way relay network with compute-and-forward in gnu radio," *Transactions on Emerging Telecommunications Technologies*, 2015.
- [26] Y. Wang and A. Burr, "Physical-layer network coding via low density lattice codes," in *European Conference on Networks and Communications (EuCNC)*, 2014.
- [27] Y. Wang, A. Burr, and D. Fang, "Complex low density lattice codes to physical layer network coding," in *ICC 2015*. IEEE, 2015.
- [28] S. Gollakota, S. D. Perli, and D. Katabi, "Interference alignment and cancellation," in *ACM SIGCOMM 2009*, vol. 39, no. 4. ACM, 2009, pp. 159–170.
- [29] C. Shepard, H. Yu, N. Anand, E. Li, T. Marzetta, R. Yang, and L. Zhong, "Argos: Practical many-antenna base stations," in *ACM MobiCom 2012*. ACM, 2012, pp. 53–64.
- [30] R. Rogalin, O. Y. Bursalioglu, H. Papadopoulos, G. Caire, A. F. Molisch, A. Michaloliakos, V. Balan, and K. Psounis, "Scalable synchronization and reciprocity calibration for distributed multiuser mimo," *IEEE Trans. Wireless Commun.*, vol. 13, no. 4, pp. 1815–1831, 2014.
- [31] Q. Yang, X. Li, H. Yao, J. Fang, K. Tan, W. Hu, J. Zhang, and Y. Zhang, "Bigstation: enabling scalable real-time signal processing in large mu-mimo systems," in *ACM SIGCOMM 2013*, vol. 43, no. 4. ACM, 2013, pp. 399–410.
- [32] S. Katti, S. Gollakota, and D. Katabi, "Embracing wireless interference: analog network coding," in *ACM SIGCOMM 2007*, vol. 37, no. 4. ACM, 2007, pp. 397–408.
- [33] M. Rizzi, M. Lipiński, T. Wlostowski, J. Serrano, G. Daniluk, P. Ferrari, and S. Rinaldi, "White rabbit clock characteristics," in *ISPCS 2016*. IEEE, 2016, pp. 1–6.
- [34] "Warp project," 2016, <http://warpproject.org>.